Electronic Supplementary Material (ESI) for Journal of Materials Chemistry C.

Widely Tunable And Anisotropic Charge Carrier Mobility In Monolayer Tin(II) Selenide Using Biaxial Strain: A First-principles Study

Mei Zhou[1,2], Xiaobin Chen[3], Menglei Li[4], and Aijun Du[5]

[1] *Institute of Applied Physics and Computational Mathematics, No.6 Garden Road, Haidian District, Beijing 100088, China*

[2] *Department of Physics and State Key Laboratory of Low-Dimensional Quantum Physics, Tsinghua University, Beijing 100084, China*

[3] *Department of Physics, Center for the Physics of Materials, McGill University, Montréal, Québec H3A 2T8, Canada*

[4] *Center for Fusion Energy Science and Technology, Chinese Academy of Engineering Physics, No.6 Garden Road, Haidian District, Beijing, China*

[5] *School of Chemistry, Physics and Mechanical Engineering, Queensland University of Technology, Brisbane, QLD 4001, Australia*

(Dated: December 20, 2016)

I. The band structure of PBE and HSE functionals

Figure S1 shows the band structures of bulk SnSe calculated with both PBE and HSE06 functionals. It can be seen that bulk SnSe is an indirect-gap semiconductor. The band gaps of bulk SnSe provided by PBE and HSE06 functionals are 0.5 eV and 1.01 eV, respectively. The latter agrees rather well with experimental value of 0.9 eV[1–3], indicating that HSE06 functional is more suitable for this system.

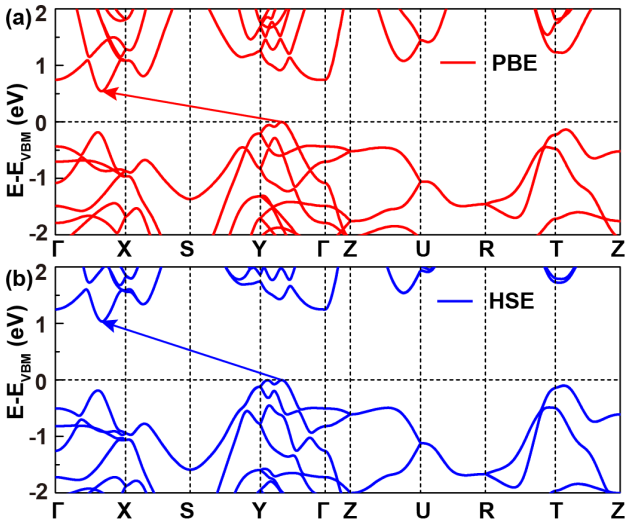

FIG. S1. (Color online) Electronic band structures of bulk SnSe calculated with PBE (a) and HSE06 (b) functionals, respectively. The Fermi level is set to the valence band maximum.

II. The cleavage energy and strength as a function of the separation distance for a fracture in bulk SnSe

To calculate the cleavage energy of bulk SnSe, a fracture is introduced in a supercell containing four SnSe layers as shown in Fig. S2, so that the distance between two fractures is more than 20 Å to avoid the artificial interactions. The fracture separation distance d is defined with respect to the interlayer separation (2.70 Å) in the equilibrium configuration. The calculated cleavage energy E_{cl} and cleavage strength σ are 0.51 J/m^2 and 2.16 GPa, respectively.

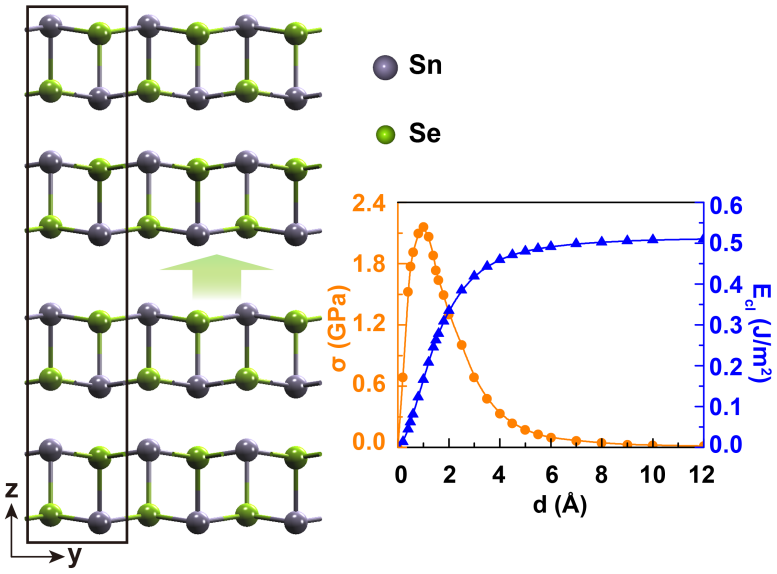

FIG. S2. (Color online) The left panel displays the cleavage of bulk SnSe. The grey and green balls denote tin and selenium atoms, respectively. The right panel presents cleavage energy E_{cl} and its derivative cleavage strength σ as a function of the separation distance d of the fracture in bulk SnSe.

III. The phonon band structure of monolayer SnSe

To check the stability of monolayer SnSe, the phonon spectrum of monolayer SnSe is calculated. There are four atoms in a unit cell, yielding twelve phonon dispersion bands (three acoustic modes and nine optical modes). As shown in Fig. S3, the frequencies of all phonon modes are positive, which confirms the dynamic stability of the single layer SnSe.

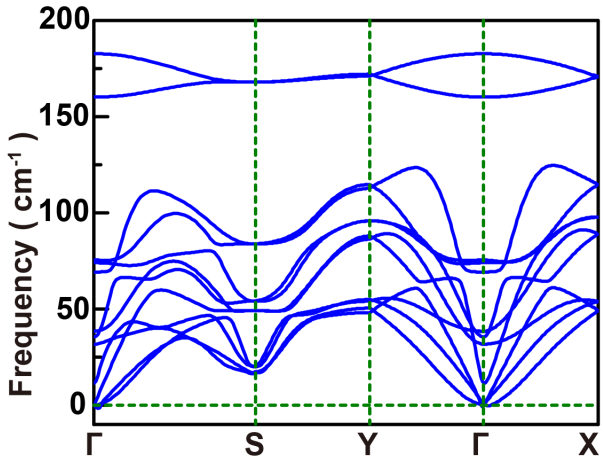

FIG. S3. (Color online) Phonon band structure for the monolayer SnSe.

IV. The electronic band structure of monolayer SnSe under 0.5% biaxial tensile strain

The calculated electronic band structure of the single layer SnSe under 0.5% biaxial strain is displayed in Fig. S4. A strong response of the CBM to external strain is observed: the CBM switches from K_2 to K_1 even with 0.5% biaxial tensile strain applying on monolayer SnSe. This indicates that monolayer SnSe is very sensitive to external strain and would transform to be a direct-gap semiconductor under a rather small biaxial strain.

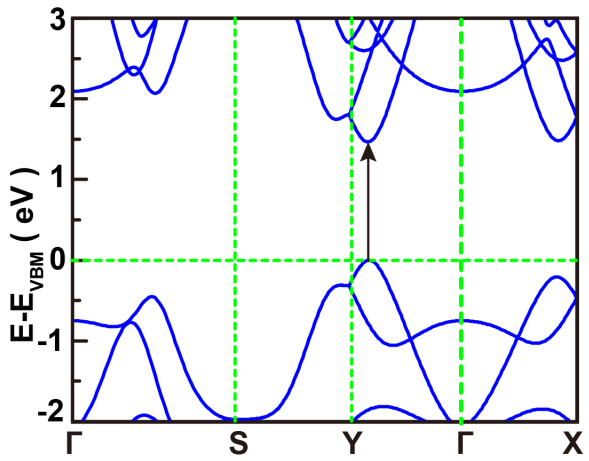

FIG. S4. (Color online) The electronic band structure of the single layer SnSe under biaxial tensile strain of 0.5%. The Fermi level is set to the valence band maximum.

V. A typical process to calculate deformation potential of biaxial strained monolayer SnSe

In our calculations of electron and hole mobilities, the deformation potential of biaxial strained monolayer SnSe is derived from linear fitting of the energies of CBM(electrons) and VBM(holes) with respect to the vacuum energy as functions of the lattice dilation along x or y directions. The deformation potential is defined as the absolute value of slope of fitting data, which usually has an unavoidable uncertainty considering the standard fitting error. Fig. S4(a) shows energies of CBM and VBM of biaxial tensile strained monolayer SnSe (2%) with

respect to the vacuum energy as a function of lattice dilation along x and y directions with a step of 0.5%. Note that, here $l_0^{'}$ (a or b) is 102% of the lattice constants l_0 (a or b) of monolayer SnSe at zero strain. We also provide fitting details for E_x of holes of strained monolayer SnSe in Fig. S5(b). The absolute value of E_x for holes is about 8.54 eV, which is shown in Table S1. Similarly, we can calculate the values of E_x and E_y for electrons, which are 6.06 eV and 0.32 eV, respectively.

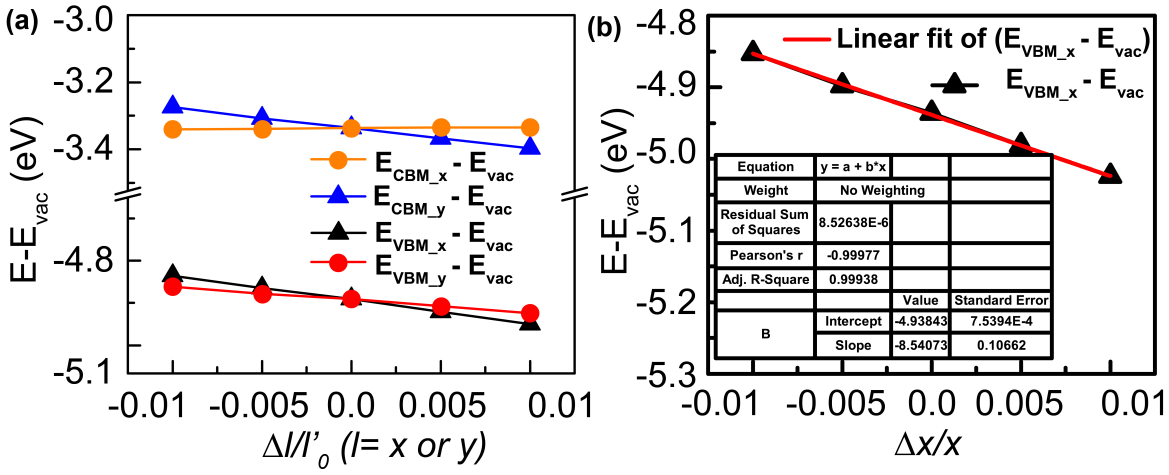

FIG. S5. (Color online) **(a) Band energy of the CBM and VBM of biaxial tensile strained monolayer SnSe(2%) with respect to the vacuum energy as a function of lattice dilations along x and y directions. (b) Fitting curves of E_{VBM} - E_{vac} as a function of lattice dilations along x direction in (a) (Red solid lines). Insets show the standard errors of the fitted slope.**

VI. The stress-strain curve of monolayer SnSe

To investigate the mechanical stability of monolayer SnSe under biaxial strain, we present stress-strain relation in Fig. S6. The ideal strength can be defined as the highest attainable stress under a uniform strain field in a defect-free crystal at zero temperature[4]. In order to compare with experimental results, the stress is scaled by h/d_0 to obtain the equivalent stress, where h is the vacuum space along the z direction for monolayer SnSe and d_0 is the effective thickness of bulk SnSe. Here the vacuum space is $h = 20$ Å and d_0 is chosen as one

half of the lattice constant along the z direction of bulk SnSe, i.e. $d_0 = 5.79$ Å. Figure S6 shows the stress-strain relation in a larger range from 0% to 20%.

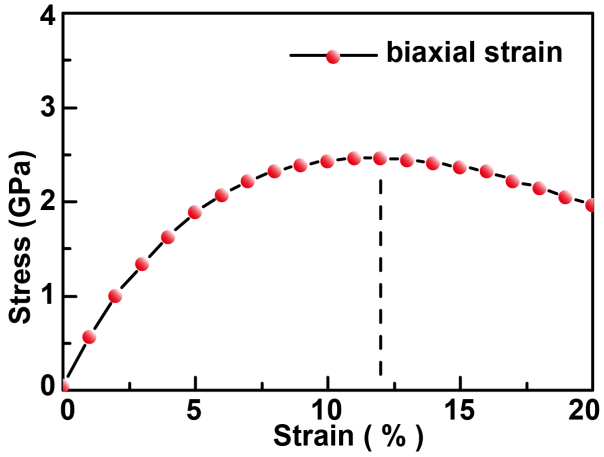

FIG. S6. (Color online) The stress-strain relation of monolayer SnSe as a function of biaxial tensile strains (red circles).

As shown in Fig. S6, the yield point of monolayer SnSe is at 12 % strain. Before this critical biaxial strain, there is the elastic range where the deformation is reversible and the stretched SnSe single layer can return to its original geometry when the tensile biaxial strain is released. After the yield point, continuous extension would induce an irreversible plastic deformation to the system and would cause a rupture after reaching the critical breaking strain eventually. For monolayer SnSe, there's no rupture within biaxial strains we considered. In a word, the above results indicate that monolayer SnSe can sustain a tensile biaxial strain about 12%.

VII. The calculated deformation potential, elastic modulus and effective masses of monolayer SnSe under various biaxial tensile strains

Table S1 shows the calculated deformation potential of electrons and holes in the single layer SnSe as a function of the biaxial tensile strain with a step of 2%. In order to figure out the singular behavior of electron mobility along the y direction, we also provide the elastic modulus and effective mass of the single layer SnSe as a function of biaxial strain with an interval of 2% in Tables S2 and S3, respectively.

TABLE S1. The calculated deformation potential of monolayer SnSe with various biaxial tensile strain.

Deformation Potential \ Strain		**0 %**	2 %	4 %	6 %	**8 %**	10 %
Location of the CBM		$\mathbf{K_2 \rightarrow K_1}$	K_1	K_1	K_1	K_1	K_1
electron (eV)	E_x	**2.56/7.04**	6.06	5.34	4.38	3.50	2.66
	E_y	**1.84/1.82**	0.32	0.26	0.52	0.77	0.99
Location of the VBM		K_1	K_1	K_1	K_1	$\mathbf{K_1 \rightarrow \Gamma}$	Γ
hole (eV)	E_x	9.20	8.54	8.13	7.09	**6.59/2.18**	2.15
	E_y	5.19	4.67	4.23	3.49	**3.04/1.10**	0.77

TABLE S2. The calculated elastic modulus of monolayer SnSe with various biaxial tensile strain.

Elastic Modulus \ Strain		**0 %**	2 %	4 %	6 %	**8 %**	10 %
C_{x_2D}	(J/m^2)	42.56	34.24	26.88	20.08	15.52	10.88
C_{y_2D}	(J/m^2)	21.44	14.08	9.12	5.12	2.40	0.32

TABLE S3. The calculated effective mass of monolayer SnSe with biaxial tensile strain.

Effective Mass \ Strain		**0 %**	2 %	4 %	6 %	**8 %**	10 %
Location of CBM		$\mathbf{K_2 \rightarrow K_1}$	K_1	K_1	K_1	K_1	K_1
electron (m_e)	m_x^*	**0.14/0.16**	0.19	0.24	0.29	0.37	0.46
	m_y^*	**0.13/0.13**	0.15	0.18	0.21	0.26	0.31
Location of VBM		K_1	K_1	K_1	K_1	$\mathbf{K_1 \rightarrow \Gamma}$	Γ
hole (m_e)	m_x^*	0.13	0.20	0.37	0.81	**0.21/1.94**	2.04
	m_y^*	0.14	0.19	0.22	0.29	**0.38/0.99**	0.93

VIII. The electronic band structure of monolayer SnSe under biaxial compressive strains

Fig. S7 displays the calculated electronic band structures of the single layer SnSe under biaxial compressive strains of -2% and -4%. With increasing biaxial compressive strain, the CBM of monolayer SnSe stays at K_2 point while VBM still locates at K_1 point, indicating that monolayer SnSe is still an indirect band gap semiconductor. The C_{K_2} moves down meanwhile with respect to V_{K_1} under biaxial compressive strains, giving rise to a shrinking indirect band gap.

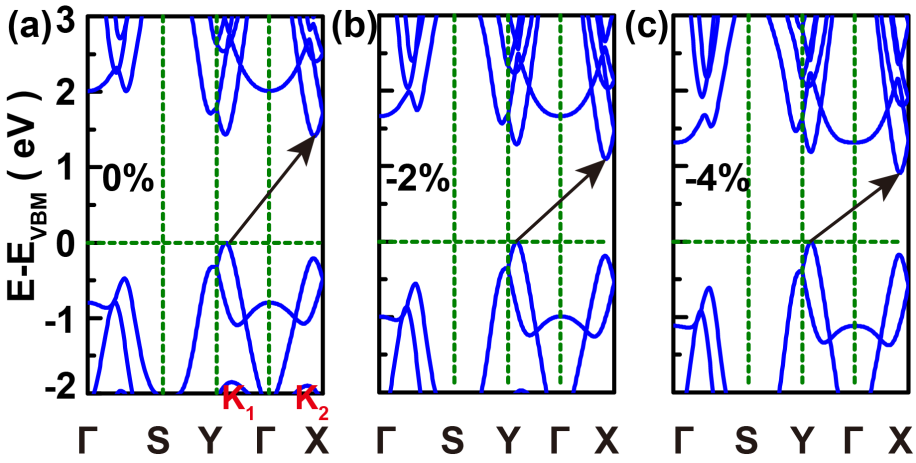

FIG. S7. (Color online) The electronic band structure of the single layer SnSe at some representative biaxial compressive strains (a) 0%, (b) -2%, (c) -4%. The Fermi level is set to the valence band maximum.

As shown in Fig.S7, the difference between C_{K_1} and C_{K_2} sees a clear increase from 0.02 eV(0%) to 0.19 eV(-2%) and to 0.28 eV(-4%). While the difference between V_{K_1} and V_{K_2} points reduces from 0.20 eV(0%) to 0.19 eV(-2%) and to 0.17 eV(-4%). According to criterion we used before, the contributions of C_{K_1} and V_{K_2} to carrier mobility can be neglected in the calculation, and only C_{K_2} and V_{K_1} are considered to perform calculations of carrier mobilities of monolayer SnSe. Another obvious change goes to the dispersion of electronic band structure of monolayer SnSe, CBs and VBs become more sharply under increasing biaxial compressive strains, suggesting a smaller effective mass than that under zero strain.

[1] H. S. Soliman, D. A. A. Hady, K. F. A. Rahman, S. B. Youssef, A. A. Elshazly, *Physica A*, 1995, **216**, 77.

[2] I. Lefebvre, M. A. Szymanski, J. O. Fourcade, and J. C. Jumas, *Phys. ReV. B* , 1998, **58**, 1896.

[3] W. J. Baumgardner, J. J. Choi, Y.-F. Lim, and T. Hanrath, *J. Am. Chem. Soc.*, 2010, **132**, 9519-9521.

[4] F. Liu, P. Ming, J. Li, *Phys. Rev. B*, 2007, **76**, 064120.